



Loss of a pyridoxal-phosphate phosphatase rescues *Arabidopsis* lacking an endoplasmic reticulum ATP carrier

Jacqueline Altensell ¹, Ruth Wartenberg,¹ Ilka Haferkamp ^{1,*†} Sebastian Hassler,¹ Vanessa Scherer ¹, Priscille Steensma ², Teresa B. Fitzpatrick ², Anurag Sharma ³, Omar Sandoval-Ibañez,³ Mathias Pribil ³, Martin Lehmann,⁴ Dario Leister ⁴, Tatjana Kleine ⁴ and H. Ekkehard Neuhaus ^{1,*†}

1 Department of Plant Physiology, University of Kaiserslautern, Kaiserslautern 67653, Germany

2 Department of Botany and Plant Biology, University of Geneva, Geneva 1211, Switzerland

3 Copenhagen Plant Science Center, University of Copenhagen, Frederiksberg 1871, Denmark

4 Department of Biology I, Ludwig-Maximilians University of Munich, Planegg-Martinsried 82152, Germany

*Author for correspondence: haferk@rhrk.uni-kl.de (I.H.), neuhaus@rhrk.uni-kl.de (H.E.N.)

†Senior authors.

T.K. performed the ethyl methanesulfonate (EMS) treatment of seeds. EMS studies were started by S.H. and finalized by J.A. T.K. supported J.A. in next-generation sequencing and corresponding data analyses. A.S., O.S.I., and J.A. performed and M.P. supervised the photosynthesis studies. V.S., J.A., and I.H. conducted functional prediction and analysis of the phosphatase, J.A. performed analyses of single and double mutants, and R.W. generated and analyzed the triple mutants. P.S. and T.B.F. conducted vitamer quantification. J.A., I.H., M.L., D.L., T.B.F., and H.E.N. discussed the data. I.H., J.A., and H.E.N. wrote the manuscript.

The author responsible for distribution of materials integral to the findings presented in this article in accordance with the policy described in the Instructions for Authors (<https://academic.oup.com/plphys/pages/general-instructions>) is: H. Ekkehard Neuhaus (neuhaus@rhrk.uni-kl.de).

Abstract

The endoplasmic reticulum (ER)-located ATP/ADP-antiporter (ER-ANT1) occurs specifically in vascular plants. Structurally different transporters mediate energy provision to the ER, but the cellular function of ER-ANT1 is still unknown. *Arabidopsis* (*Arabidopsis thaliana*) mutants lacking ER-ANT1 (*er-ant1* plants) exhibit a photorespiratory phenotype accompanied by high glycine levels and stunted growth, pointing to an inhibition of glycine decarboxylase (GDC). To reveal whether it is possible to suppress this marked phenotype, we exploited the power of a forward genetic screen. Absence of a so far uncharacterized member of the HaloAcid Dehalogenase (HAD)-like hydrolase family strongly suppressed the dwarf phenotype of *er-ant1* plants. Localization studies suggested that the corresponding protein locates to chloroplasts, and activity assays showed that the enzyme dephosphorylates, with high substrate affinity, the B₆ vitamer pyridoxal 5'-phosphate (PLP). Additional physiological experiments identified imbalances in vitamin B₆ homeostasis in *er-ant1* mutants. Our data suggest that impaired chloroplast metabolism, but not decreased GDC activity, causes the *er-ant1* mutant dwarf phenotype. We present a hypothesis, setting transport of PLP by ER-ANT1 and chloroplastic PLP dephosphorylation in the cellular context. With the identification of this HAD-type PLP phosphatase, we also provide insight into B₆ vitamer homeostasis.

Introduction

Nucleotides represent building blocks of DNA and RNA may activate metabolic precursors during polymer production and act as cofactors in enzymatic reactions or as second messengers in signal cascades (Roux and Steinebrunner, 2007; Geigenberger et al., 2010; Möhlmann et al., 2014). Among the different nucleotides, ATP plays a central role because it is the major energy currency of the cell. It acts as cosubstrate in a multitude of different reactions and thus is required in almost every cell compartment. However, in most eukaryotes, ATP regeneration from ADP and phosphate mainly takes place in mitochondria. Consequently, ATP has to be transported from the site of its production to the compartment where needed (Klingenberg, 1989). ADP/ATP carriers (AACs), the most abundant transporters in the inner mitochondrial membrane, catalyze the export of ATP, supplying the cytosol and, indirectly, other organelles with mitochondrial energy (Millar and Heazlewood, 2003). The concomitant ADP import provides one substrate for oxidative phosphorylation, whereas the second substrate (inorganic phosphate) enters the mitochondrion via specific phosphate carriers.

Besides mitochondrial energy metabolism, plants can regenerate high amounts of ATP in chloroplasts during photosynthesis. Therefore, chloroplasts appear energetically quite independent since photosynthetic ATP provides the energy for anabolic processes in the stroma. Heterotrophic plastids, however, rely on ATP uptake from the cytosol and the same holds true for chloroplasts in the night or during phases of limited photosynthetic activity (Tjaden et al., 1998; Reiser et al., 2004; Reinhold et al., 2007). The corresponding import is catalyzed by members of the major facilitator superfamily, the so-called nucleoside triphosphate transporters (NTTs) (Winkler and Neuhaus, 1999; Haferkamp et al., 2011). Interestingly, NTT-mediated ATP uptake occurs in exchange with ADP and phosphate, and thus energy provision to the plastid enables the subsequent export of the two products of energy consumption (Trentmann et al., 2008).

The endoplasmic reticulum (ER) harbors several energy-demanding processes such as protein folding, protein maturation, and protein quality control, but lacks the capacity for ATP regeneration (Guillén and Hirschberg, 1995). Therefore, this organelle essentially relies on the ATP uptake from the cytosol (Mayinger and Meyer, 1993). Although substantial ATP passage across the ER membrane was demonstrated as early as 1992 (Clairmont et al., 1992), the molecular nature of the corresponding facilitator protein remained unknown for a long time.

In 2008, an ATP/ADP antiporter was identified in the ER of *Arabidopsis thaliana* (ER-ANT1) and thus could be considered as the first promising candidate. Structurally, this protein represents a homolog to the mitochondrial AACs and catalyzes, when recombinantly expressed in *Escherichia coli*, the exchange of ATP and ADP (Leroch et al., 2008). The corresponding gene shows increased expression in organs and tissues with high protein

folding activity in the ER, and loss-of-function mutants (*er-ant1*) exhibit decreased transcription of ATP-dependent ER enzymes, as well as less lipid and storage proteins in seeds (Leroch et al., 2008). These observations tempted us to speculate that ER-ANT1 proteins, which have been identified at the molecular level in the representative mono and dicotyledonous plants, rice (*Oryza sativa*) and *Arabidopsis*, respectively, fulfill functions in energy metabolism and ATP dependent processes in the ER lumen (Leroch et al., 2008; Zhang et al., 2016). However, several later observations suggest that ER-ANT1 does not represent the universal long-sought major ATP supplier of the ER because energy provision to the lumen is required in all eukaryotes, but ER-ANT1 homologs are restricted to vascular plants (Haferkamp and Schmitz-Esser, 2012; Hoffmann et al., 2013). Thus, even in the absence of ER-ANT1 sufficient ATP supply to the ER is guaranteed, and is accordingly mediated by an alternative transport system (Leroch et al., 2008; Hoffmann et al., 2013).

In fact, recent studies identified ATP/ADP exchanger in the ER membrane (AXER) as the major ATP/ADP exchanger in this organelle in mammalian cells (Klein et al., 2018). The corresponding protein belongs to the solute carrier family and is not an AAC-type protein. It was shown that this ATP/ADP exchanger is of high relevance for the ER energy metabolism and homologs to AXER exist in all eukaryotes, including plants (Klein et al., 2018). Thus, since AXER catalyzes the main ATP provision to the ER the exact physiological function of ER-ANT1 is unknown. Moreover, from an evolutionary point of view it is hard to envision why a mitochondrial AAC homolog was recruited to the ER to deliver ATP (given the subsequently established function of AXER) and, in addition, it is unclear why solely vascular plants would possess two different types of ATP/ADP transporters.

However, independent of the exact physiological role of ER-ANT1, its importance for the plant is beyond doubt (Leroch et al., 2008). This is, because *Arabidopsis er-ant1* knock-out lines (*er-ant1*) exhibit a dwarf phenotype and decreased chlorophyll levels when grown at ambient CO₂ concentrations (Leroch et al., 2008). Moreover, *er-ant1* mutants accumulate the photorespiratory key-intermediate glycine, are impaired in CO₂ fixation, and exhibit a higher CO₂ compensation point than wild-types (wts; Hoffmann et al., 2013), which are typical characteristics for many photorespiration mutants (Bauwe et al., 2010). Furthermore, while *er-ant1* *Arabidopsis* and rice mutants suffer severely under ambient air, they are rather unaffected under conditions of high CO₂ availability (Hoffmann et al., 2013; Zhang et al., 2016), which is also consistent with other photorespiratory mutants (Bauwe et al., 2010).

Thus, the current data suggest that ER-ANT1 may at least contribute to the energy metabolism of the ER and fulfills a specific role in vascular plants that is somehow connected to photorespiration. However, although the different enzymatic steps of the photorespiratory pathway are distributed among several cellular compartments, none are associated with the ER membrane or its lumen

(Timm et al., 2016). Therefore, the link between ER-mediated adenine nucleotide transport, catalyzed by ER-ANT1, and the photorespiratory phenotype of the loss-of-function mutant remains enigmatic.

To shed light on the plant-specific function of ER-ANT1 and how its absence might affect photorespiration we conducted a suppressor screen of *er-ant1*. Alleviation of the growth defect of the ER-ANT1 loss-of-function mutant could be achieved by knocking out the activity of a further protein, namely a putative HaloAcid Dehalogenase (HAD)-like hydrolase. Interestingly, the latter protein specifically acts on pyridoxal 5'-phosphate (PLP), identifying the HAD-like hydrolase as a PLP phosphatase (PLPP). Further studies demonstrate that changes in the concentration of PLP are causative for the *er-ant1* phenotype and localization experiments revealed that this protein locates in chloroplasts. The analyses conducted lead to the hypothesis that ER-ANT1 influences subcellular B₆ vitamers levels, connecting an ER-located PLP reserve to the rest of the cell. In addition, we provide evidence for an active dephosphorylation of PLP in chloroplasts which contributes to vitamin B₆ homeostasis.

Results

Suppressor mutants of *er-ant1* are phenotypically diverse

To gain further insights into the properties of *er-ant1* mutants, we conducted mutagenesis of *er-ant1* plants with ethyl methanesulfonate (EMS). The resulting M₁ plants were grown in pools of ~500 plants to produce the M₂ generation of seeds. The progeny was screened for putative suppressors of the *er-ant1* phenotype (termed *ser-ant1*). For this, M₂ seeds were cultivated at ambient air on soil for 3 weeks and then screened visually for plants substantially larger than *er-ant1*. This strategy led to the identification of several putative *ser-ant1* mutants. False positives were excluded by confirmation of the *er-ant1* T-DNA insertion and after self-pollination of the isolated M₂ *ser-ant1* mutants, we used 13 lines of the M₃ generation for further characterization and mapping.

During visual inspection of these M₃ plants, it became directly evident that the individual *ser-ant1* lines differ in terms of rosette size, coloration, and shape of leaves (Figure 1A). This heterogeneous appearance is suggestive of genetic variations among the different lines. Although all selected M₃ *ser-ant1* mutants were larger, appeared greener, and developed more leaves than *er-ant1* mother plants, they did not reach the wt level. Solely line 16.2 was almost as large and as green as wt, but showed a more pronounced leaf serration. Line 1.3 was only slightly larger than *er-ant1* plants, whereas the remaining lines exhibited intermediate sizes. The young leaves in the center of the rosette of several *ser-ant1* lines were of normal green coloration, while older leaves appeared comparatively pale. The young leaves of line 6.3 appeared even darker green than those of wt. Line 5.4 had strikingly yellow cotyledons, whereas line 4.2 was

generally very pale and, in this context, highly resembled the phenotype of *er-ant1* mutants.

To analyze whether the apparent suppression of chlorosis in the different lines becomes reflected by an increase in chlorophyll per fresh weight (FW), we quantified this pigment in the *ser-ant1* lines, *er-ant1*, and the wt (Figure 1B). Generally, the chlorophyll content of *er-ant1* is low and makes up only about a third of wt levels. Notably, all tested *ser-ant1* lines show higher chlorophyll contents when compared with *er-ant1*. They reached at least 50% of the wt level and five of the selected 13 lines even approach it ($\geq 90\%$ of wt). Interestingly, the chlorophyll content of the smallest line 1.3 represents the lowest among the *ser-ant1* mutants, while the chlorophyll level of line 16.2 is nearly identical to that of wts. Therefore, suppression of the *er-ant1* growth defect is generally accompanied by an increase in chlorophyll. However, even though their chlorophyll content was almost fully recovered many plants were still substantially smaller than the wt.

Suppressor mutants exhibit better photosynthetic performance than *er-ant1*

Previous analyses revealed that *er-ant1* is substantially impaired in photosynthesis (Hoffmann et al., 2013). Its limited photosynthetic capacity is presumably causative, or at least contributes to the growth retardation typical for this mutant plant. To check whether suppressor lines not only contain more chlorophyll but also show higher photosynthetic capacities than *er-ant1*, we determined their maximum quantum yield of photosystem II (PSII), represented by (F_v/F_m). For this, we selected two suppressor lines (no. 8.3 and no. 1.2) exhibiting almost complete recovery of the chlorophyll contents, namely 80%–90% of the wt level. We detected no significant differences between the F_v/F_m values of the wt, *er-ant1*, and the two suppressor lines when plants were cultivated under high CO₂ (Figure 2A). Their F_v/F_m values were at ~0.83 (Figure 2A) which is indicative of unstressed plants (Demmig and Björkman, 1987).

Exposure to ambient CO₂ conditions for 5 d did not alter the maximum quantum yield of PSII in the wt. However, a significant decrease of the maximal quantum yield became apparent in *er-ant1* mutants (F_v/F_m ~0.74; Figure 2B) whereas the two suppressor lines were less affected (F_v/F_m ~0.8). The improved growth of the suppressor lines thus can be attributed to their increased chlorophyll contents and higher photosynthetic capacities when compared with *er-ant1*.

Suppressor mutants still accumulate glycine

Another striking characteristic of *er-ant1* is its marked glycine accumulation in leaves (Hoffmann et al., 2013). Since some *ser-ant1* lines show restored growth and chlorophyll contents, as well as improved photosynthesis, we were interested in whether they accumulate less glycine than *er-ant1* mutants. Interestingly, not only did *er-ant1* plants contain approximately about 70-fold more glycine than the wt plants, but all tested *ser-ant1* lines also accumulated

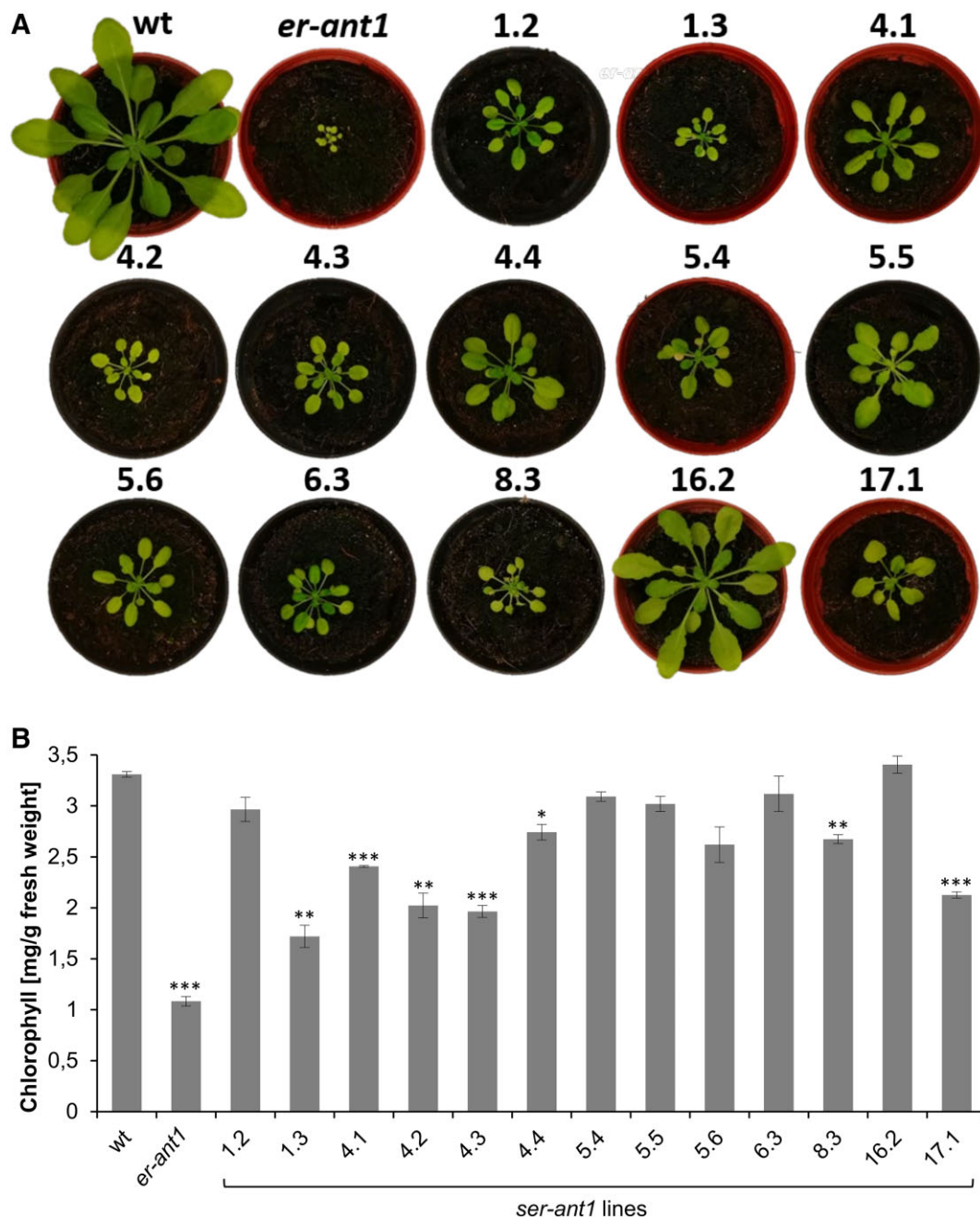


Figure 1 Suppression of the *er-ant1* phenotype by *ser-ant1* mutations. A, Suppressor mutants selected for further characterization and mapping. Photographs show representative 28-d-old third-generation (M_3) plants for each selected mutant line, plants were grown on soil at ambient air. Images were digitally extracted for comparison. B, Total chlorophyll content in leaves of *er-ant1* and M_3 *ser-ant1* plants relative to the wt. Mean values of three individual replicates \pm SE. Asterisks indicate the significance level between wt and mutant plants according to a Student's *t* test (* $P < 0.05$, ** $P < 0.01$, *** $P < 0.001$).

substantial amounts of this amino acid. Their glycine concentration was at least 30-fold higher than in wt plants and several plants even contained as much glycine as in the original *er-ant1* mutant (Figure 3).

Identification of *ser-ant1* loci

To identify the suppression causing mutations in individual *ser-ant1* lines, we used the mapping-by-sequencing approach

(James et al., 2013). To this end, the homozygous *ser-ant1* lines were backcrossed (BC_1) individually with the parental *er-ant1* T-DNA insertion line that was used for generating the EMS suppressor mutant collection. The fact that all individuals of the BC_1 - F_1 progeny displayed the dwarf *er-ant1* phenotype, whereas the BC_1 - F_2 progeny segregated in a 1:3 ratio of *ser-ant1*- to *er-ant1* phenotypes suggests that the suppressor mutations are recessive. After self-pollination, the

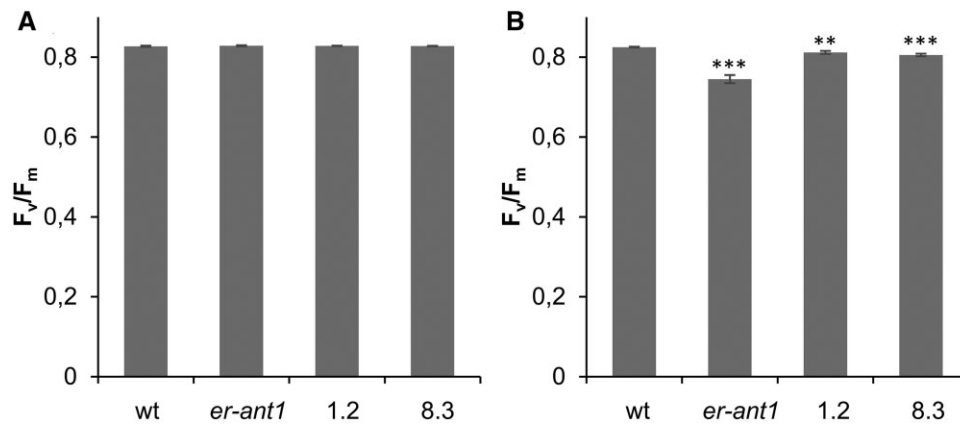


Figure 2 Maximum quantum yield of PSII (F_v/F_m) of wt, *er-ant1*, and two selected M3 *ser-ant1* plants. A, F_v/F_m at 2,000 parts per million (ppm) CO₂. B, F_v/F_m at ambient air. Data represent mean values of seven individual replicates, \pm SE. Asterisks indicate the significance level between wt and mutant plants according to a Student's *t* test (** $P < 0.01$, *** $P < 0.001$).

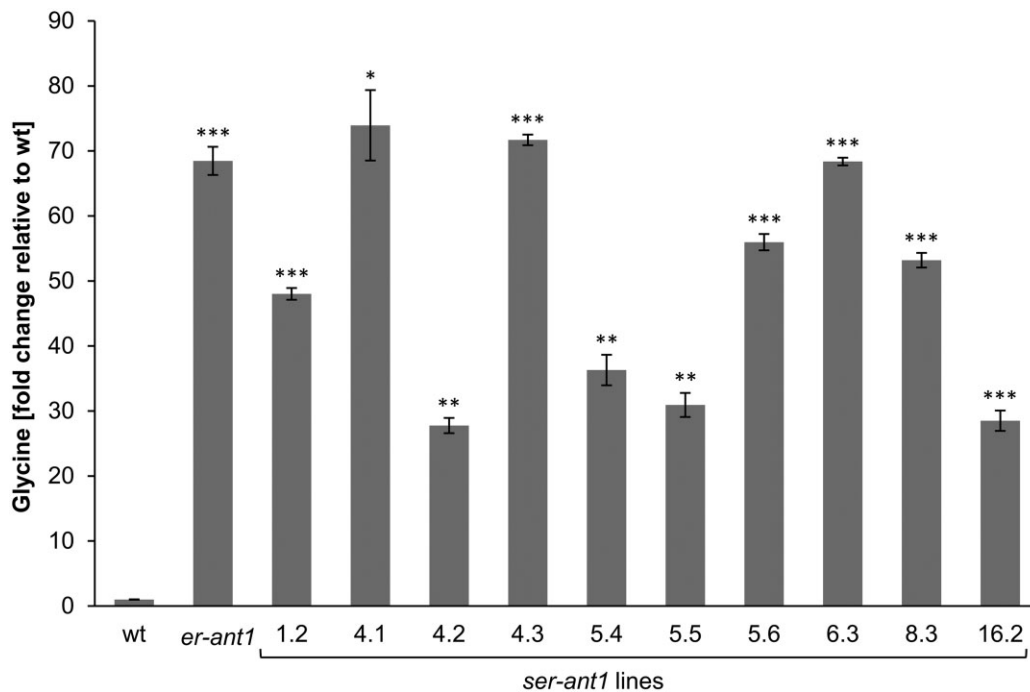


Figure 3 Glycine content of leaves from *er-ant1* and *ser-ant1* mutants relative to the wt level. Plants were cultivated at ambient CO₂ conditions. The glycine content of the wt was set to 1. Data represent mean values of five individual replicates \pm SE. Asterisks indicate the significance between the glycine levels of wt and mutant plants according to a Student's *t* test (* $P < 0.05$, ** $P < 0.01$, *** $P < 0.001$).

BC₁-F₂ segregating populations (~500 plants per line) were analyzed for the *ser-ant1* phenotype. Subsequently, two bulked pools of plants per line displaying either the *ser-ant1*- or the *er-ant1* phenotype were created, each consisting of 50 individuals. Pooled genomic DNA from each bulk was sequenced with average depths in the range of 41× to 56×. The fragmented sequences were mapped to the reference genome (Arabidopsis TAIR10) and the identified EMS mutation variants were analyzed (and filtered) to exclude noncausative mutations. By analyzing the allelic variant frequencies (AFs) it became clear that nine *ser-ant1* lines carry the suppression causing mutation in a specific region at

chromosome 2. Interestingly, seven of these lines possessed the highest AFs for variants in the genetic information of *At2g33255* (Supplemental Table S1). Therefore, we considered mutations in this gene as the most promising candidate suppressors. In line 6.3, the mutation resulted in a premature stop codon, which suggests that the alleviation of the *er-ant1* phenotype is due to activity loss of the corresponding protein (Supplemental Figure S1). To rule out that the identified single-nucleotide polymorphism (SNP) in *At2g33255* is a false-positive, the mutation was checked by Sanger-sequencing of *gDNA* from individuals of the 6.3 M₃ generation (Supplemental Figure S2).

Confirmation of the candidate suppressor mutations in *At2g33255* by reverse genetics

We used reverse genetics to investigate whether loss of function of the *At2g33255* encoded protein is causative for the observed phenotype suppression. For this, three individual *At2g33255* T-DNA insertion lines were ordered and by the help of reverse transcription-quantitative PCR (RT-qPCR) we verified that two of them (termed *had1-2* and *had1-3*, see below) represent true loss-of-function (knock out) mutants, whereas one (*had1-1*) still contained almost 50% of the wt transcript level (Supplemental Figure S3A). Morphologically, *had1-2* and *had1-3* were indistinguishable from wt plants (Supplemental Figure S3B). We used the *had1-2* line for crossing with *er-ant1*. When cultivated under ambient CO₂ levels, the segregating F₂ progeny exhibited either the *had1-2* (wt like) phenotype, the original *er-ant1* (dwarf) phenotype, or an intermediate size (semi-size) phenotype (Figure 4A). Using a T-DNA screen confirmed that exclusively the semi-sized plants were homozygous for T-DNA insertions in both the *er-ant1* and the *At2g33255* gene. Subsequently, homozygous F₃-plants were analyzed for expression of the *At2g33255* gene by RT-qPCR (Figure 4B). The absence of the corresponding transcript demonstrates that the semi-sized plants represent true *had1-2* × *er-ant1* double knockouts (Figure 4B). This observation demonstrates that absence of the *At2g33255* transcript alleviates the growth defect of *er-ant1*. To further confirm that the absence of HAD1 activity is causative for alleviating the dwarf phenotype, we reintroduced the active HAD1 by expression of the wt *HAD1* gene under either the constitutive ubiquitin promoter or the endogenous *HAD1* promoter, named *ubiq::HAD1* × *had1-2* × *er-ant1* and *promHAD1::HAD1* × *had1-2* × *er-ant1*, respectively (Supplemental Figure S4). Several homozygous *ubiq::HAD1* × *had1-2* × *er-ant1*- and *promHAD1::HAD1* × *had1-2* × *er-ant1* triple mutant lines exhibited increased *HAD1* mRNA, appeared morphologically

markedly smaller and showed pale leaves (Supplemental Figure S4, A and B), as is typical for the original *er-ant1* line (Figure 4A; Leroch et al., 2008).

At2g33255 encodes a PLPP

Although the T-DNA insertion in *At2g33255* was proven as causative to suppress dwarf growth of *er-ant1* mutants (Figure 4A) the physiological background for this finding was completely unclear, particularly because the function of the corresponding enzyme is unknown. The protein encoded by *At2g33255* is annotated as a member of the HAD-like superfamily (HADSF). Generally, the HADSF comprises proteins with a conserved α/β -domain, which shares similarity with the Rossmann fold and is termed “hydrolase fold” (Burroughs et al., 2006). Interestingly, different from the implication of its name, the HADSF consists predominantly of phosphatases (~79%) and ATPases (~20%), whereas dehalogenases as well as phosphonates, phosphomutases, and phosphomannomutases represent the minority of the protein superfamily members (Koonin and Tatusov, 1994; Kuznetsova et al., 2015).

Within the HADSF the protein encoded by *At2g33255* belongs to the HAD subfamily IA. Representatives of this subfamily are characterized by a small α -helical cap between loop 1 and loop 2 of the core domain. In Arabidopsis, the HADSF subfamily IA is formed by 19 proteins (IPR006439) (Krishnakumar et al., 2014; Mitchell et al., 2018) and 7 of these proteins have been characterized as phosphatases (Caparrós-Martín et al., 2013). Therefore, it appeared likely that *At2g33255* also encodes a phosphatase. Phosphatases are generally not very substrate-specific and often accept various phosphorylated substrates. However, a previous screen by others using D,L-glycerol-3-phosphate, D-fructose-6-phosphate, D-fructose-1-phosphate, D-fructose-1,6-bisphosphate, D-glucose-6-phosphate, α -D-glucose-1-phosphate, 2-deoxy-D-glucose-6-phosphate, D-mannose-6-phosphate, or

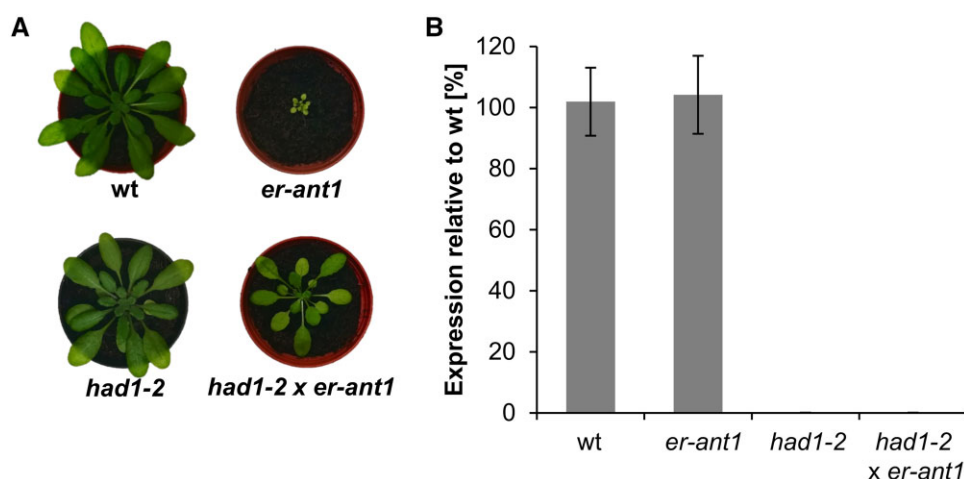


Figure 4 Absence of the *At2g33255* transcript suppresses the growth defect of *er-ant1*. A, Phenotypic comparison of 4 weeks old plants grown at ambient CO₂. Images were digitally extracted for comparison. B, *At2g33255* gene expression analyzed by RT-qPCR. RNA for cDNA synthesis was extracted from leaves of 3 weeks old plants. Data were normalized to the SAND (*At2g28390*) housekeeping gene. Data represent mean values of three biological replicates ± SE.

α -D-mannose-1-phosphate failed to detect any phosphatase activity of the *At2g33255* gene product (Caparrós-Martín et al., 2013).

To get an idea about its possible function, we used its predicted amino acid sequence for NCBI Blast searches (<https://blast.ncbi.nlm.nih.gov/Blast.cgi>) against nonplant genomes. Interestingly, we identified high similarities to the YOR131C-like HADSF members from *Saccharomyces cerevisiae* (baker's yeast). YOR131C was identified as a PLPP (Kuznetsova et al., 2015). Due to the considerable amino acid similarity of the predicted protein sequence of *At2g33255* to YOR131C (44%; Figure 5), we hypothesized that it might also exhibit hydrolytic activity against PLP.

Subcellular localization of the *At2g33255* encoded protein

The N-terminal extension of the amino acid sequence of *At2g33255*, when compared with the yeast homolog (Figure 5), points to a mitochondrial or plastidic targeting of the encoded protein. This putative localization is supported by in silico prediction programs, however, with quite moderate reliability scores. Thus, to clarify the ambiguous localization we transiently expressed the *At2g33255* sequence in either *Nicotiana benthamiana* or Arabidopsis protoplasts as a translational fusion to green fluorescent protein (GFP), either at the N or the C terminus. Protoplast transformation with the C-terminally attached marker protein resulted in weak green fluorescence surrounding the position of the chloroplast. The strongest signal intensity, however, was

detectable in the center of the organelle (Figure 6) indicating accumulation of the GFP fusion protein in the stroma. With GFP attached to the N-terminus, the fluorescence signal of the fusion protein was distributed throughout the cell but not detectable in chloroplasts (Figure 6). This observation suggests that the N-terminally attached GFP masks the chloroplast targeting signal of the HAD-type hydrolase and by this hinders its entry into the organelle.

The uncharacterized HAD-type hydrolase from Arabidopsis acts as a PLPP

The sequence similarities between the yeast PLPP (YOR131C) and the HAD-type hydrolase are (Figure 5) indicative of a related enzymatic activity. To gain insights into the biochemical properties of the HAD-type hydrolase from Arabidopsis, the protein was heterologously expressed in *E. coli*, purified to apparent homogeneity via immobilized metal affinity chromatography (IMAC; Supplemental Figure S6) and subsequently used in enzymatic activity tests.

Interestingly, in the presence of PLP, we observed measurable phosphate release. The generation of free phosphate increased nearly linearly with time and reached values of about 3.9 $\mu\text{mol mg protein}^{-1} \text{h}^{-1}$ (Figure 7A). Omitting magnesium (Mg^{2+}) from the test medium substantially decreased phosphate release (Figure 7B) and no enzymatic activity was detectable when PLP was absent (Figure 7B). Similarly, use of heat-denatured enzyme or lack of enzyme in the test only led to background levels of phosphate release (Figure 7B). These observations demonstrate that (1)

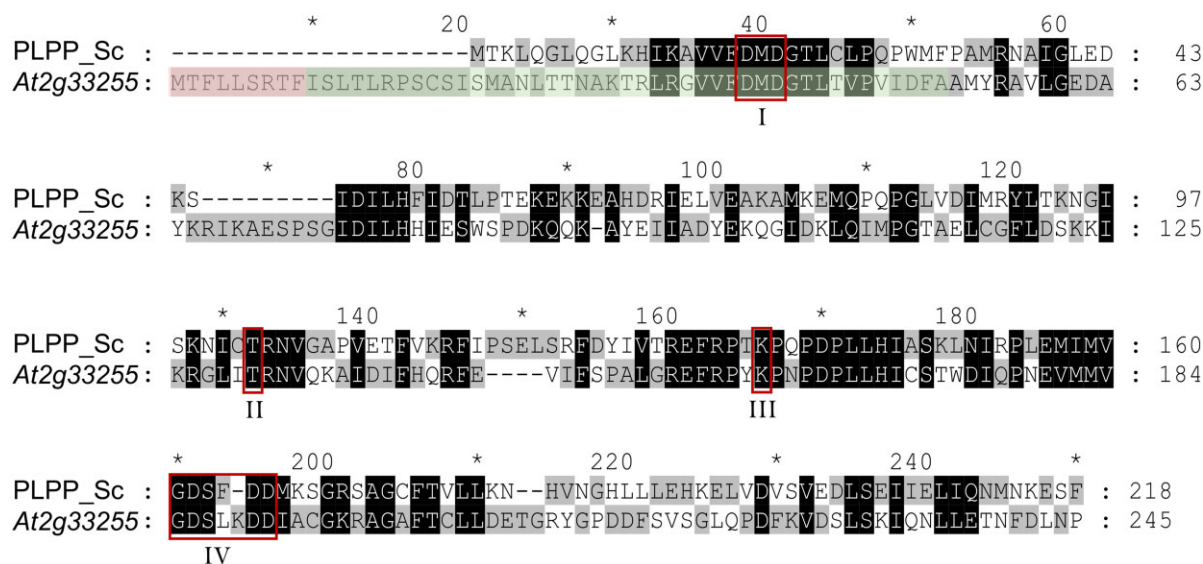


Figure 5 ClustalW alignment of the amino acid sequences of the PLPP from *S. cerevisiae* (PLPP_Sc; YOR131C) and the *At2g33255* gene product. Residues identical among the two sequences or with similar properties are indicated by black shading. Residues not identical are highlighted by different shading (gray/white). Red boxes mark conserved HADSF motifs I–IV (I: DxD; II, T/S; III: K/R; IV: E/DD, GDxxD, or GDxxxxD). The putative mitochondrial targeting sequence (according to TargetP) is shaded in red. The predicted chloroplast targeting sequence (according to ChloroP) comprises also the green shaded residues. Dashes represent introduced gaps for alignment improvement. Numbers at the right indicate amino acid positions. The amino acid sequence alignment also demonstrates that the *At2g33255* encoded protein is N-terminally extended by 20 residues when compared with the cytosolically located PLPP YOR131C from *S. cerevisiae*. Such extensions often act as targeting sequences signifying the import of proteins into mitochondria or chloroplasts. Notably, the *At2g33255* encoded protein does not share substantial sequence similarity (25%) to a recently identified chloroplastic PLP phosphatase from *N. tabacum*, named *NtPLPP1* (ShuoHao et al., 2019; Supplemental Figure S5).

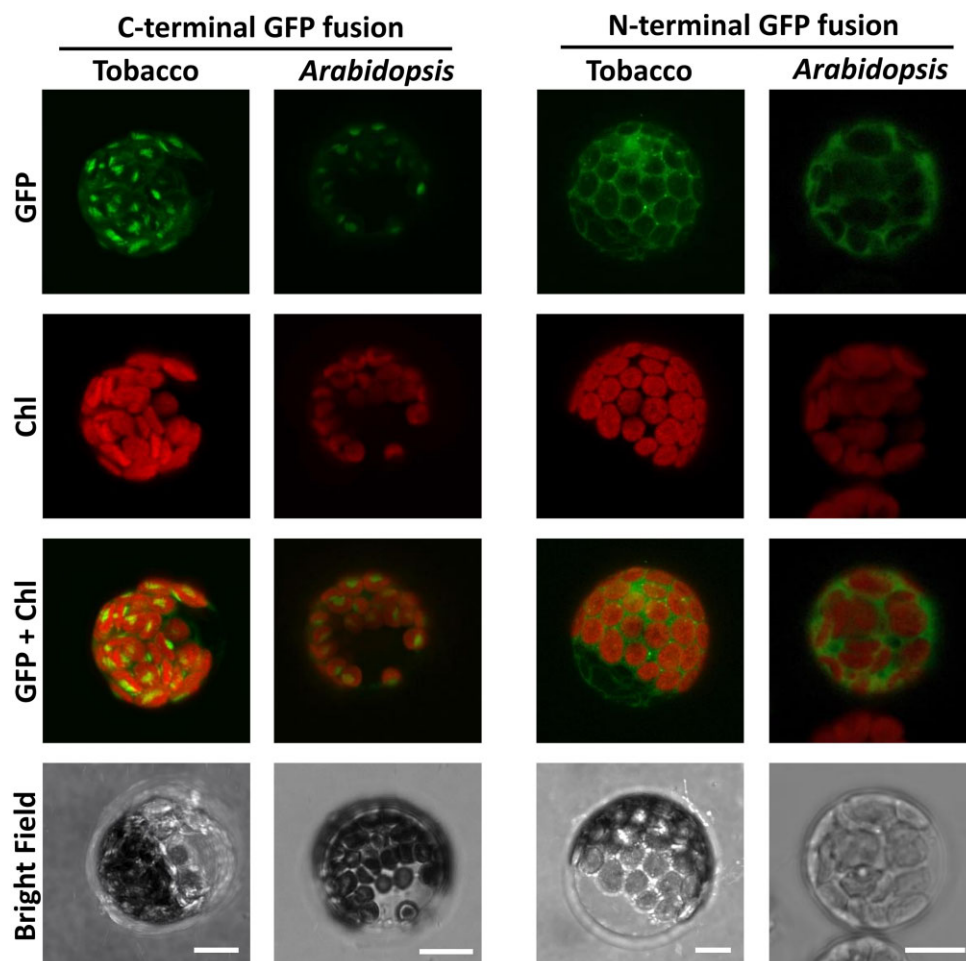


Figure 6 Localization of the HAD-type hydrolase in *N. benthamiana* and *Arabidopsis* protoplasts. Pictures were taken with a confocal laser-scanning microscope 16 h after transient transformation. Scale bars = 10 μm . Chl, chlorophyll fluorescence.

phosphate release depends on the activity of the recombinant protein, (2) phosphate is released from PLP, and (3) the enzyme activity depends markedly upon the presence of Mg^{2+} , which is a typical feature of HADSF-type phosphatases (Kuznetsova *et al.*, 2015). Because of the PLPP activity, we term the HAD-type hydrolase At2g33255 from now on AtPLPP1.

A previous study failed to detect any hydrolytic activity of the At2g33255 encoded enzyme with nine different substrates (Caparrós-Martín *et al.*, 2013), pointing to a notable substrate specificity of the protein. However, it is important to mention that PLP was not among the previously tested compounds (Caparrós-Martín *et al.*, 2013). The fact that we could observe phosphate release from PLP shows that the recombinant enzyme is active, which is an important prerequisite for the investigation of its substrate preference. Therefore, we checked whether the AtPLPP1 exhibits hydrolytic activity toward a range of other phosphorylated compounds (Table 1). Six of the 13 tested metabolites did not serve as substrates. All other compounds tested showed < 10% of the phosphate release observed when using PLP as substrate (Table 1), with the exception of ATP (30.5%). These observations support the conclusion that At2g33255

acts as a AtPLPP1. We also analyzed the rate of phosphate release as a function of the PLP concentration allowing us to determine an apparent K_m value of 30 μM , and a V_{max} of the purified protein of 0.123 $\mu\text{mol mg protein}^{-1} \text{min}^{-1}$ (Figure 7C, inset therein).

Indications for a perturbed B_6 vitamers metabolism in *er-ant1*

The group of B_6 vitamins is composed of six vitamers: pyridoxal (PL), pyridoxine (PN) and pyridoxamine (PM), and their phosphorylated forms PLP, PNP, and PM 5'-phosphate (PMP) (Fitzpatrick *et al.*, 2007; Hellmann and Mooney, 2010). PLP, acting as an essential coenzyme for a wide range of enzymes, can be biosynthesized *de novo* in the cytosol (Tambasco-Studart *et al.*, 2005). Salvage pathways allow for interconversion of the different vitamers (Parra *et al.*, 2018) and are distributed throughout the cellular organelles (Rueschhoff *et al.* 2012; Colinas *et al.*, 2016).

Here, the localization studies suggest that AtPLPP1 is targeted to the chloroplast (Figure 6). Consequently, absence of this enzyme would decrease the rate of PLP hydrolysis in the stroma and by this could increase PLP availability in this organelle. The observed suppression of dwarfism by activity

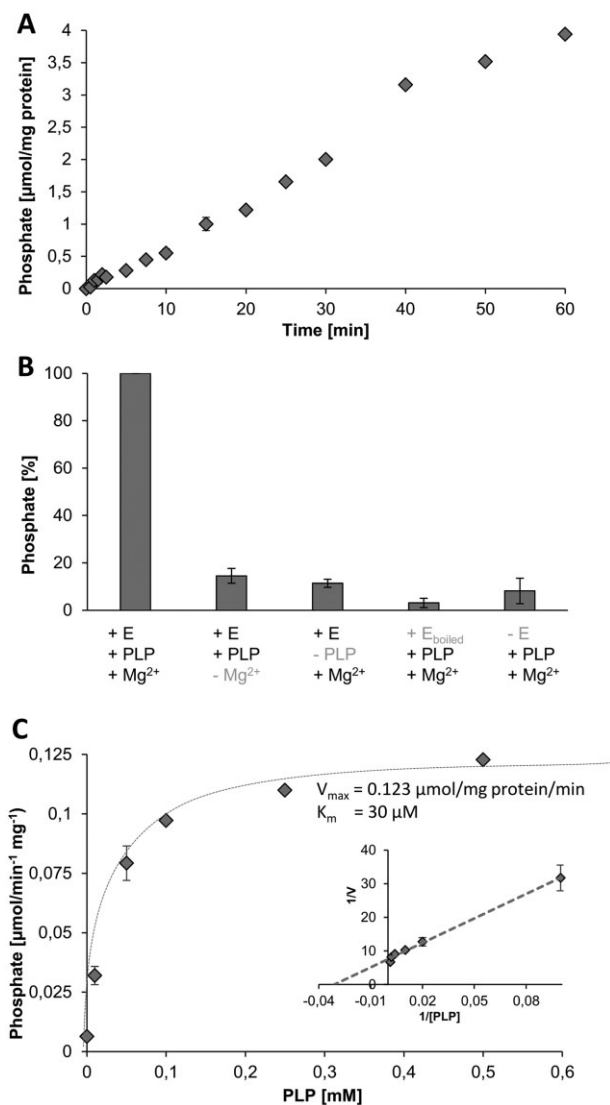


Figure 7 Enzyme assays verified the PLPP function of the At2g33255 encoded protein. A, Time course of phosphate release from PLP (0.2 mM). B, Phosphate release is dependent on the active enzyme (+ E), presence of PLP (0.2 mM), and Mg^{2+} . Each assay time was 30 min. C, Michaelis–Menten curve indicating substrate saturation of enzyme activity, the inset shows a corresponding Lineweaver–Burk analysis indicating an apparent K_m for PLP of $30 \mu M$ and a V_{max} of $0.123 \mu mol mg\ protein^{-1} min^{-1}$. Each assay time was 30 min. Shown are mean values of four replicates \pm SE.

loss of the AtPLPP1 might thus point to a perturbed cellular B_6 vitamer metabolism in *er-ant1* mutant plants that is alleviated by PLP availability.

If this hypothesis is true, exogenously supplied B_6 vitamers might be beneficial for mutant development. To test this assumption, we cultivated *er-ant1* and wt seedlings on agar plates supplemented with increasing concentrations of the B_6 vitamer PN. In this context, it is important to note that solely nonphosphorylated B_6 vitamers can enter the cell (Rueschhoff et al., 2012) and that PN supplements B_6 vitamin metabolism since it can act as a precursor for PLP generation (Rueschhoff et al., 2012). The feeding assay revealed

Table 1 Enzymatic activity of At2g33255 on different putative substrates

Tested substrate	Phosphate release as %
6-phosphogluconic acid	n.d.
D-Fructose-6-phosphate	n.d.
D-Fructose-1,6-bisphosphate	n.d.
D-Glucose-6-phosphate	3.5
α -D-glucose-1-phosphate	n.d.
Glyceraldehyde 3-phosphate	n.d.
3-Phosphoglyceric acid	6.5
Dihydroxyacetone-phosphate	9.0
Phosphoenolpyruvate	n.d.
Adenosine triphosphate	30.5
Adenosine diphosphate	1.8
Adenosine monophosphate	3.2
PLP	100.0

Notes: Assays were performed with 1 mM substrate and $6.25 \mu g$ of the recombinant phosphatase per 0.5 mL. A colorimetric change of the assay mix indicated release of phosphate after 30 min of incubation at $23^\circ C$. n.d., not detectable $\leq 1\%$.

that the growth of wt seedlings remained unaltered by PN additions up to 1 mM (Figure 8A). However, the highest PN concentration used (5 mM) had a negative impact on growth of the wt seedlings and led to a substantial decrease in biomass ($< 50\%$ of the corresponding control, 0 mM PN, Figure 8B). In contrast, *er-ant1* seedlings grew much better in the presence of PN supplementation. Their size and biomass increased with rising PN concentrations (Figure 8, A and B) and the highest PN concentration tested resulted in almost three-fold higher biomass of the *er-ant1* seedlings when compared with the corresponding control (0 mM PN; Figure 8B). This stimulatory effect of PN feeding on seedling growth is thus indicative for limiting levels of the essential vitamin B_6 in *er-ant1* plants.

Except for glycine levels, the simultaneous loss of AtPLPP1 function largely restores the perturbed amino acid metabolism of *er-ant1* mutants

Although alleviated in growth, the *ser-ant1* mutants accumulate high amounts of glycine (Figure 3). The glycine content of line 6.3, with the premature stop codon in the At2g33255 gene, was even identical to that of *er-ant1* (Figure 3). To check whether this is also true for the *had1-2 x er-ant1* double knock-out mutant, we quantified its glycine concentration and compared it with that of the wt and the two single knock-out plants. Moreover, we additionally determined the concentrations of all amino acids already known to be markedly altered in *er-ant1* when compared with the wt (Hoffmann et al., 2013). The amino acid content in *had1-2* and *had1-3* generally resembled those of the wt (Table 2). As previously reported, besides its high glycine accumulation *er-ant1* plants exhibit particularly high arginine (Arg) content, whereas the levels of aspartate (Asp), glutamate (Glu), and alanine (Ala) are substantially lower than present in wt leaves (Table 2). Interestingly, the absence of AtPLPP1 in *er-ant1* (*had1-2 x er-ant1* suppressor mutant plants) did not markedly reduce the glycine accumulation

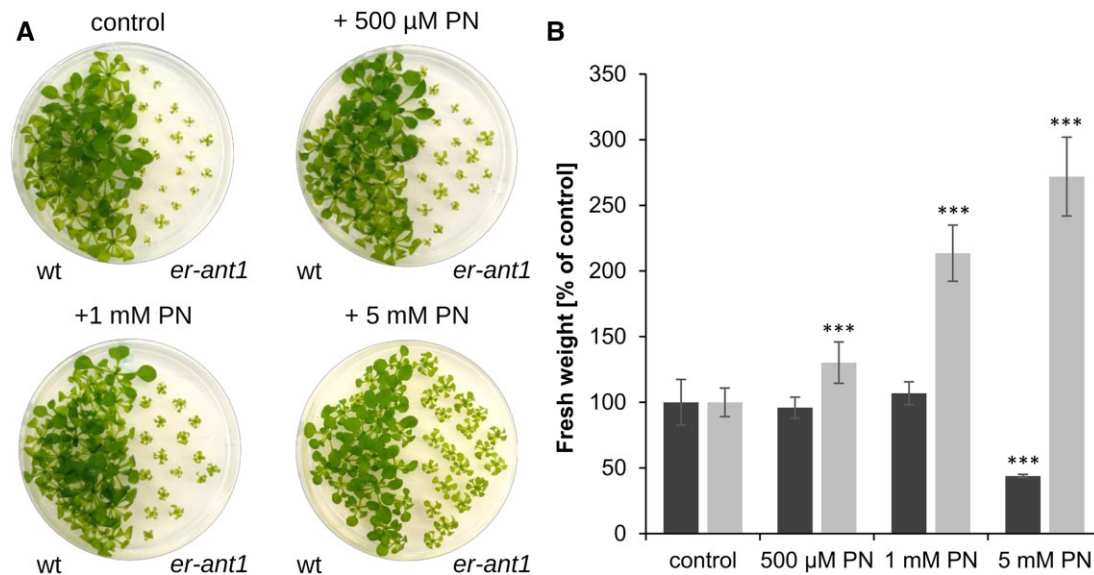


Figure 8 Effect of PN feeding on growth of *er-ant1* and wt plants. Twenty plants were cultivated on agar plates (0.5 MS including GAS vitamins, 0.8% agar) at ambient CO₂ conditions (10-h light/14-h dark) for 25 d. A, wts and *er-ant1* plants on agar plates without additional PN (control) and with different concentrations of additional PN. B, FW of *er-ant1* (light gray) and corresponding wt plants (dark gray) grown on agar plates containing different concentrations of PN. The FW is given as a percentage of the respective control FW. Shown are mean values of at least five individual plates \pm SE. Asterisks indicate the significance level between wt and mutant plants according to a Student's *t* test (***) $P < 0.001$.

Table 2 Altered amino acid contents of *had1-2*, *had1-3*, *er-ant1*, and *had1-2 x er-ant1* mutants when compared with wt plants

Amino acid	<i>had1-2</i> (%)	<i>had1-3</i> (%)	<i>er-ant1</i> (%)	<i>had1-2 x er-ant1</i> (%)
Asp	95	98	12***	93*
Glu	104	93	24***	82*
Glycine	158	102	6,847***	6363***
Ala	115	104	20***	96
Arg	109	122	847***	124

Notes: Plants were grown at 2,000 ppm CO₂ for 4 weeks and subsequently shifted to ambient air for 5 d. Samples were taken on the fifth day, 5 h after onset of light. Shown are the mean values of four individual replicates. The obtained concentrations were normalized to the respective wt concentration (set to 100%). Asterisks indicate the significance levels between wt and mutants according to a Student's *t* test.

* $P < 0.05$,
*** $P < 0.001$.

but restored the remaining amino acid concentrations to almost wt levels (Table 2).

Arg can be taken as an indicator for the plant nitrogen status (Winter et al., 2015). It appeared remarkable that *er-ant1* plants contained ~ 8.5 times more Arg when compared with wt, while the corresponding levels in mutant lines *had1-2* and *had1-3*, as well as in the double mutant *had1-2 x er-ant1* resembled wt concentrations (Table 2).

Insights into vitamin B₆ metabolism of the different mutant plants

The data of this study led us to the conclusion that the HAD-type hydrolase acts as a PLPP in chloroplasts of Arabidopsis and that *er-ant1* mutants might suffer from imbalanced B₆ vitamers homeostasis (Figures 7 and 8). To

identify possible changes in B₆ vitamers contents, we determined the levels of PMP, PLP, PM, PN, and PL in wt-, single- and double-knockout plants (Figure 9, A and B).

The levels of the low abundant B₆ vitamers PM and PN range between 100 and 250 pmols g Fw⁻¹ and are similar in all five plant lines analyzed (Figure 9A). Assuming that the newly identified AtPLPP1 dephosphorylates PLP it is not surprising that both HAD loss-of-function lines, *had1-2*, and *had1-3*, contained significantly increased PLP levels when compared with wt (Figure 9A). The corresponding levels of PL and PMP in both *had1* mutants closely resembled wt concentrations (Figure 9A). *er-ant1* mutants showed decreased PLP levels when compared with wts, while both PL and PMP concentrations were again similar to the corresponding concentrations found in wt (Figure 9A). The sum of all B₆ vitamers in *had1-2* plants is slightly increased, but decreased in *er-ant1* plants when compared with the corresponding levels in wt (Figure 9B).

Discussion

Although ER-ANT1 was biochemically characterized more than a decade ago (Leroch et al., 2008) and although corresponding loss-of-function plants have been analyzed in detail (Hoffmann et al., 2013), the exact cellular role of this transporter remains elusive. It is particularly unclear how impaired ER-ANT1 activity in the membrane of the ER causes a defect in photorespiration, since a connection between these two processes was not evident. Thus, to gain deeper insights into the metabolism of the *er-ant1* mutant and to enlighten the possible link between ER-ANT1 and photorespiration, we made use of the power of an EMS-based forward-genetic screen. By this approach, we identified a

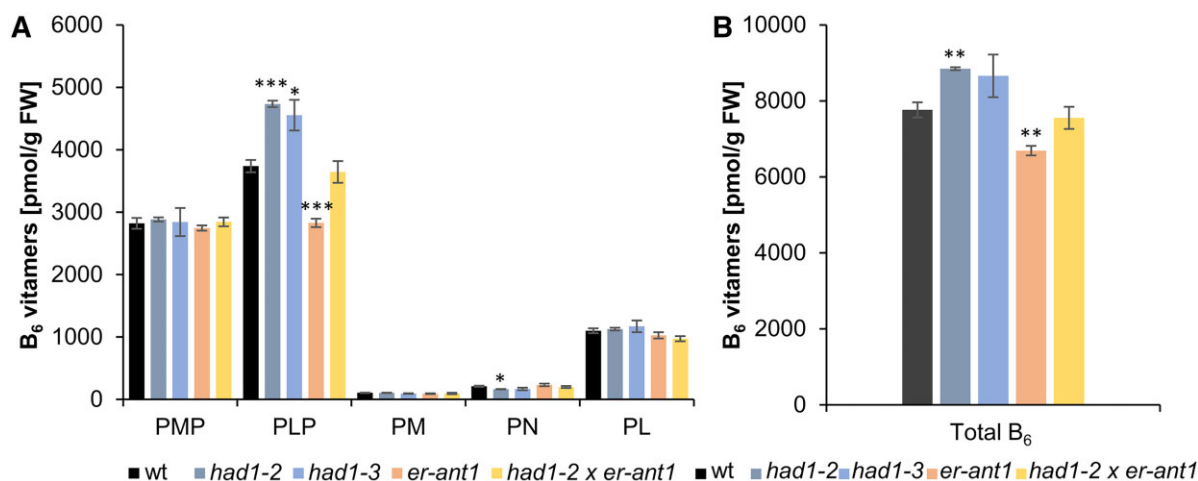


Figure 9 Analysis of the B₆ vitamers contents in the different plant lines. A, Analysis of the individual B₆ vitamers PMP, PLP, PM, PN, and PL profile of the lines as indicated. B, Total vitamers contents (sum of PMP, PLP, PM, PN, and PL). Plants were grown at high CO₂ (2,000 ppm) for 33 d to avoid pleiotropic effects on B₆ vitamers in dwarf type *er-ant1* plants. Data represent the mean of four replicates per line that was used for two extractions each. SEs are given. Statistical relevance was determined by a Student's *t* test using the wt of the respective growth condition as a reference: **P* ≤ 0.05, ***P* ≤ 0.005, and ****P* ≤ 0.0005.

promising candidate mutation suppressing the marked growth defect of *er-ant1* (Figure 1 and Supplemental Table S1). The corresponding gene variant led to a premature stop codon in a putative HAD-type hydrolase (Supplemental Figures S1 and S2), which suggests that loss of this enzyme activity suppresses the *er-ant1* phenotype (Figures 1 and 3). In fact, subsequent reverse genetics confirmed that loss of the HAD-type phosphatase is causative for suppression of the dwarf growth typical for *er-ant1* mutants (Figure 4 and Supplemental Figure S4, A and B).

Despite the positive outcome of the EMS screen, it was initially unclear why the missing activity of a putative HAD-type hydrolase exhibits suppressor function, since its subcellular localization and biological function were unknown. However, GFP-based studies on both *N. benthamiana* and Arabidopsis protoplasts were indicative for its location in the chloroplast stroma (Figure 6), which concurs with the presence of a putative organellar targeting-sequence extension at the N-terminal end of this protein, and which is absent from the structural homolog YOR131C from baker's yeast (Figure 5). The affiliation of the enzyme to the HAD-type hydrolase superfamily suggested that it acts as a phosphatase, since most members of this protein group exhibit phosphatase activity (Burroughs et al., 2006). Moreover, the considerable amino acid sequence similarity of this protein to the PLPP YOR131C from baker's yeast (44%; Figure 5; Kuznetsova et al., 2015) strongly supported the assumption of a related biochemical function in Arabidopsis chloroplasts. This assumption was supported by the positive effect of the PLP precursor PN on growth of *er-ant1* mutants (Figure 8) suggesting that PLP was lacking in the latter mutants.

Accordingly, enzyme assays revealed that this HAD-type phosphatase is a functional and PLP-specific phosphatase (Table 1). The marked Mg²⁺ dependency of this enzyme

(Figure 7B) supports to some degree its stromal location as the concentration of Mg²⁺ is high in chloroplasts when compared with all other plant cell organelles (Karley and White, 2009). However, Mg²⁺-dependent enzymes are not restricted to chloroplasts and we cannot rule out that a fraction of this novel enzyme locates outside the chloroplast, as corresponding GFP signals might be too weak to be detected.

That the newly identified protein is not only functional in enzyme activity tests (Figure 7, A and B) but also in planta was then confirmed by analyzing the B₆ vitamers levels in both wt and loss-of-function plants. These analyses showed that the two independent *had1* loss-of-function lines (*had1-2* and *had1-3*) exhibit significantly increased PLP concentrations when compared with wts (Figure 9A). Therefore, it can be concluded that this enzyme hydrolyzes PLP not only in vitro but also in planta, and that its activity in chloroplasts contributes to the control of cellular PLP levels and with this to B₆ vitamers homeostasis. Accordingly, we assign the name PLPP1 to this protein from Arabidopsis (*AtPLPP1*). In this context, it is important to mention that a recent study identified an alternative PLPP in chloroplasts of *Nicotiana tabacum* (*NtPLPP*), which similar to *AtPLPP1* exhibits marked Mg²⁺ dependency (ShuoHao et al., 2019). Thus, it is likely that the presence of chloroplast-located PLPP enzymes extends to other vascular plants.

The recombinant *AtPLPP1* exhibits an apparent *K_m* for PLP of 30 μM (Figure 7C), which represents ~15 times higher substrate affinity to that reported for *NtPLPP* (0.45 mM, see ShuoHao et al., 2019). A phylogenetic analysis indicates that Arabidopsis harbors a homolog to *NtPLPP* (ShuoHao et al., 2019), which, however, has so far not been characterized. Thus, it remains elusive whether two independent chloroplastic PLPPs are active in Arabidopsis. An answer to this question not only depends upon the respective

substrate affinity but also upon the level of the enzyme in chloroplasts which is unknown. In any case, the markedly high affinity of AtPLPP1 for PLP is fully in line with the low concentration of this vitamer in Arabidopsis (Fitzpatrick et al., 2007; González et al., 2007).

It has been shown previously that the dwarf growth of *er-ant1* mutants corresponds to a photorespiratory phenotype (Hoffmann et al., 2013). This phenotype is apparently caused by an inhibition of the activity of glycine decarboxylase (GDC; Hoffmann et al., 2013), representing an essential enzyme complex involved in photorespiration and locating to the mitochondrial matrix (Bauwe et al., 2010; Timm et al., 2012). Since *er-ant1* plants exhibit a high accumulation of glycine, when compared with wts (Table 2; Hoffmann et al., 2013) and because glycine accumulation can be prevented under conditions of high CO₂ (Hoffmann et al., 2013), which also abolishes the dwarf growth of *er-ant1*, it was speculated that the considerable glycine accumulation on the mutant line might cause impaired plant development (Hoffmann et al., 2013). However, here in this study, given that the suppressor mutant *had1-2 x er-ant1* contains nearly identical glycine levels as observed in *er-ant1* mother plants (64- and 68-fold increase, respectively; Table 2), we can now conclude that such high glycine levels in Arabidopsis are not the direct cause for the *er-ant1* dwarf phenotype. This statement is consistent with observations on transgenic GDC knock-down dosage potato mutants exhibiting even up to 100-fold higher glycine levels as present in the wt, but are still viable and able to produce tubers (Heineke et al., 2001). So far it is unclear whether *had1-2 x er-ant1* mutants show less unfolded protein response (UPR), which is a typical characteristic of *er-ant1* loss-of-function mutants as revealed in both Arabidopsis and rice (Hoffmann et al., 2013; Zhang et al., 2016). Interestingly, to the best of our knowledge modified PLP levels have not been connected to UPR in the ER. However, the *had1-2 x er-ant1* mutants might serve as a starting point to conduct future corresponding experiments.

Thus, the metabolic origin for the phenotypic peculiarity of the dwarf growth of *er-ant1* must be due to something else. Quantification of amino acids known to be markedly altered in *er-ant1* (Hoffmann et al., 2013) revealed that the cellular concentrations of Asp, Glu, and Ala, while strongly decreased in leaves of *er-ant1*, approach wt levels in *had1-2 x er-ant1* plants (Table 2; Hoffmann et al., 2013). The biosynthesis of all three amino acids starts in chloroplasts and is dependent upon the activity of the enzymes Glu/2-oxo-glutarate amino transferase (GOGAT), as well as on Ala and Asp aminotransferases (Reyes-Prieto and Moustafa, 2012). Although all three enzymes use specific substrates, they share the conserved amino acid transferase property which is dependent upon the coenzyme PLP (Eliot and Kirsch, 2004). Therefore, given that (1) AtPLPP1 resides in chloroplasts (Figure 6), that (2) *er-ant1* plants suffer from low PLP levels (Figure 9A), and that (3) *had1* loss-of-function mutants show increased PLP levels (Figure 9A) while *had1-2 x er-ant1* plants exhibit PLP as well as Asp, Glu, Arg, and Ala

concentrations similar to wts (Figure 9A; Table 2), we propose that the restoration of the stromal PLP levels are causative for the marked suppression of the *er-ant1* dwarf phenotype.

It is worth to mention that the decrease of Asp, Glu, and Ala levels in *er-ant1* mutants is specific and is not simply due to the sequestration of NH₄⁺ in the high pool of glycine (Table 2). This is because the *had1-2 x er-ant1* suppressor plants exhibit similarly increased glycine levels as observed in *er-ant1*, but show Asp, Glu, and Ala concentrations similar to wt (Table 2). Moreover, *er-ant1* plants also exhibit markedly increased levels of Arg (Table 2) and the latter amino acid is generally a specific indicator for a high cellular NH₄⁺ availability (Sato and Yanagisawa, 2014; Winter et al., 2015). In fact, our assumption that limited amino acid transferase activity due to PLP deprivation in the stroma is causative for the *er-ant1* dwarf phenotype under ambient CO₂ is further supported by the observation that these mutants grow like the wt under high CO₂ conditions (Hoffmann et al., 2013).

It is known that a high metabolic flux through the photorespiratory pathway (which is suppressed under high CO₂) leads to a remarkable release of NH₄⁺ at the mitochondrial GDC (Douce et al., 2001). The chloroplastic enzyme couple of glutamine synthase and Glu synthase (GOGAT) is mandatory for reassimilation of NH₄⁺ which is released during photorespiration (Keys, 2006). The low GDC activity in *er-ant1* plants, which is ~40% of that in wts, is not caused by a decrease of the corresponding protein level (Hoffmann et al., 2013). Thus, it was speculated in a latter study that, besides an inhibitory glutathionylation of GDC, the GDC activity in *er-ant1* is limited by further unknown factors (Hoffmann et al., 2013). Given that low PLP levels limit chloroplast located PLP dependent reactions (Table 2), we propose that the GDC activity in *er-ant1* mitochondria is also inhibited by insufficient availability of PLP in corresponding mesophyll cells. This assumption is supported by the fact that GDC belongs to the most abundant enzymes in plant cells, representing about one-third of all mitochondrial proteins (Oliver et al., 1990), and that therefore its demand for PLP is relatively high.

Since *had1-2 x er-ant1* suppressor mutants develop similarly to wt plants (Figures 1 and 4A) but still contain high glycine levels, the question arises: why does a stromal increase in PLP not rescue the GDC activity in mitochondria? An answer to this might be that although the absence of the newly identified AtPLPP1 leads to increased stromal PLP levels (Figure 9A) this vitamer is most likely not able to pass the chloroplast envelope (Rueschhoff et al., 2012). Thus, even if a PLP carrier protein exists in plant mitochondrial membranes, as is the case in mitochondria of yeast and mammals (Lui et al., 1981, 1982; Whittaker et al., 2015; Parra et al., 2018), the restored stromal PLP levels in *had1-2 x er-ant1* plants do not communicate with the surrounding cytosol.

A hypothesis of how ER-ANT1 might affect the PLP availability in plant cells

The data above show that metabolic disturbances in the chloroplast caused by impaired PLP homeostasis in *er-ant1* mutants can be suppressed by knocking out *AtPLPP1*. Thus, as a final question, we have to ask: how might a carrier protein residing in the ER membrane affect plant PLP homeostasis?

For a hypothesis setting ER-ANT1 into the scene of PLP homeostasis, we first have to recall that the ER of vascular plants harbors many specific functions in, for example lipid metabolism, cell-to-cell communication, or osmotolerance (Galili et al., 1998; Barton et al., 2011; Corso et al., 2018), which are absent in other eukaryotes. Moreover, the plant ER lumen harbors an impressive number of solutes, in particular solutes of low concentrations, which fulfill essential functions in signaling and stress responses typical for and restricted to plant cells (Helliwell, 2006; Friml and Jones, 2010; Wulfetange et al., 2011; Ju et al., 2012; Oda et al., 2016). Accordingly, the presence of ER-ANT1, which is solely found in vascular plants but not in other eukaryotes (Hoffmann et al., 2013; Zhang et al., 2016), is in line with the specific functions of the plant ER.

Given that ER-ANT1 is acting as a counter exchanger (Leroch et al., 2008) and in line with all the data above we propose that a fraction of cellular PLP in vascular plants locates to the ER lumen and is exported via ER-ANT1, in counter exchange with cytosolic ATP. Thus, in *er-ant1* mutants, a low cytosolic PLP level prevents its uptake into mitochondria, leading to an impaired GDC activity (Hoffmann et al., 2013; Table 2). As another result of this PLP scavenging, the cytosol will probably also contain low PL levels, which subsequently limit stromal PLP synthesis by chloroplast located enzyme SOS4 kinase (Rueschhoff et al., 2012). The observation that ATP import into *E. coli* cells expressing ER-ANT1 is not inhibited by PLP (Leroch et al., 2008) does not argue against our assumption since it is unknown whether PLP is able to pass the outer bacterial membrane, or whether a specific orientation of ER-ANT1 in the *E. coli* membrane prevents access of PLP to the binding site.

We are fully aware that this hypothesis needs further experimental evaluation, but we are also fully aware that upcoming analyses which are from now on possible on *had1-2* × *er-ant1* plants as well as on the other so far not further analyzed suppressor mutants (Figures 1 and 3) will in future allow to clarify why the absence of ER-ANT1 activity causes the marked phenotype in corresponding loss-of-function mutants.

Materials and methods

Plant material and growth conditions

Studies were performed with *Arabidopsis* (*A. thaliana*) ecotype Columbia-0 wt plants, T-DNA insertion mutants with an insertion in *At5g17400* (*er-ant1*: SALK_043626) (Leroch et al., 2008), EMS mutagenized *er-ant1* plants of the *M*₃-generation and T-DNA insertion mutants with an insertion in

At2g33255 (*plpp*: SALK_041216C verified with primer pairs—*plpp*_LP: TCAAAGCAGAGAGCCCTAGTG, *plpp*_RP: GCTATGGAGAAAGGGTTGACC; *plpp-2*: SAIL_871_G11 verified with primer pairs—*plpp-2*_LP: TTGCATACACCAGATTTTGCTC, *plpp-2*_RP: ATCAGACGAAAACCCAAATCC). Before germination, seeds were incubated for 2 d in the dark at 4°C on standardized ED73 soil (Weigel and Glazebrook, 2002). If not stated otherwise, plants were grown diurnally for 10 h at 22°C and 120 μmol photons m⁻² s⁻¹ light intensity followed by 14 h at 18°C without light. Plants were either grown at ambient CO₂ levels (~400 ppm) or high CO₂ levels (2,000 ppm) in Fitotron plant climate chambers (Weiss Technik, Reiskirchen, Germany). For cultivation in sterile culture, seeds were surface sterilized (5 min 70% EtOH, 10 min 5% sodium hypochlorite for 10 min followed by washing three times with ddH₂O) and subsequently stratified in water for 2 d at 4°C in the dark, before transfer to sterile 0.5 MS agar plates (0.2203% MS salts incl. vitamins, 0.5% [w/v] sucrose, 0.05% [w/v] MES, pH 5.7 [KOH], 0.8% [w/v] plant agar).

EMS mutagenesis and suppressor screen and construction of a mapping population

About 125,000 *er-ant1* seeds were mutagenized by incubation in 0.4% (vol/vol) EMS solution for 8 h as previously described (Kim et al., 2006). The resulting *M*₁ plants were grown and allowed to self-pollinate in pools of ~500 plants at 2,000 ppm CO₂ on soil. *M*₂ seeds of the individual pools were grown at ambient CO₂ conditions on soil. After 3 weeks, individual suppressors of the *er-ant1* phenotype (*ser-ant1*) *M*₂ plants were allowed to self-pollinate. The *er-ant1* background of the *M*₃ generation was ensured by verifying the presence of the T-DNA-insertion in *At5g17400* (*er-ant1*) by PCR (Leroch et al., 2008).

BSA and NGS

To identify mutations causative for the suppression, bulked segregant analysis (BSA) was combined with whole-genome next-generation sequencing (NGS), similar to previously described by Song et al. (2017). For the generation of mapping populations, *M*₃ mutants were backcrossed with individuals of the parental *er-ant1* line. The resulting *F*₁ generations were allowed to self-pollinate. Subsequently, the individual segregating *F*₂ generations were used for mapping. For each investigated suppressor line, gDNA was extracted and pooled from rosette leaves of 50 plants with a *ser-ant1* phenotype (positive pool) and from 50 plants showing the *er-ant1* phenotype (negative pool). gDNA extraction was performed as previously described (Pallotta et al., 2000). The pooled gDNA samples of 13 mapping populations and pooled gDNA of 50 original *er-ant1* mutant plants were used for NGS. The whole-genome resequencing and bioinformatic data analysis of the raw NGS data were provided by Novogene (Beijing, China). Briefly, the genomic DNA was randomly sheared into fragments of ~350bp and subjected to library construction using the “Illumina TruSeq Library Construction Kit” (Illumina, San Diego, CA, USA) according

to the manufacturer's instructions. After library quality control, 150-bp paired-end sequencing was performed on the "Illumina HiSeq" platform (Illumina). Image files were firstly transformed to sequence reads by base calling with CASAVA software (version 1.8; Illumina). The sequencing quality was assessed using FastQC Phred score evaluation. Adapters as well as low-quality reads were removed. The effective sequencing data were aligned to the reference sequence TAIR10 (ftp://ftp.Arabidopsis.org/home/tair/Genes/TAIR10_genome_release/) through BWA software and duplicates were removed with SAMtools (Li et al., 2009). To evaluate the similarity between each sample and the reference genome, mapping statistics such as mapping rate, average sequencing depth, and coverage were evaluated. SNPs were detected with SAMtools. To reduce the error rate in SNP detection, results were filtered, so that only SNPs were taken into account with more than four supporting reads and a mapping quality >20. Candidate SNPs were identified by SNP ratio mapping and the application of Candi-SNP (Etherington et al., 2014) and were verified via Sanger sequencing.

RNA isolation

Rosette leaves were harvested and ground in liquid nitrogen. Total RNA was isolated from 50 mg of the triturated material using the "NucleoSpin RNA Plant Kit" according to the manufacturer's instructions (Macherey & Nagel, Düren, Germany). The RNA concentration was determined by photometric measurement at a nanodrop machine (Peqlab, Erlangen, Germany).

RT-qPCR

From total RNA, mRNA was transcribed into cDNA with reverse transcriptase (Verso-Kit, Thermo Fisher Scientific, Karlsruhe, Germany). For determining the expression of *AtPLPP1*, "PerfeCTa SYBR Green" was used according to the manufacturer's instructions (Quantabio, Gaithersburg, MD, USA) with the following primer combination: PLPP_qRT_fwd: GAGTCCTGATAAACAGCAGAAGGC and PLPP_qRT_rev: AGCCACATAGTTCAGCAGTACCAG. For normalization, *SAND* (At2g28390) was used as a housekeeping gene (*SAND*_qRT_fwd: AACTCTATGCAGCATTGATC CACT, *SAND*_qRT_rev: TGATTGCATATCTTTATCGC CATC). Amplification and fluorescence detection were performed using a MyiQ iCycler (Bio-Rad, Munich, Germany). Relative quantification was performed using the $2^{-\Delta\Delta C_t}$ method (Livak and Schmittgen, 2001).

Chlorophyll quantification and photosynthetic measurements

Rosette leaves for chlorophyll determination were harvested and ground in liquid nitrogen. Extinctions of leaf extracts at the red absorption maxima of Chl_a (~663 nm) and Chl_b (~646 nm) were measured and total chlorophyll content was determined (Porra, 2002). To investigate PSII performance via PAM analysis, plants were dark adapted for 15 min prior to exposure to actinic light. The effective PSII

quantum yield, $Y(II)$, was measured and calculated according to Genty et al. (1989).

Quantification of amino acids

Rosette leaves were harvested and ground in liquid nitrogen. An aliquot of 500 μ L water was added to 100 mg of triturated material and the mixture was shaken for 15 min at 99°C (600 rpm). The starch and cell debris were sedimented by centrifugation at 20,000 $\times g$. For the measurement, 20 μ L of the sample supernatant was mixed with 60 μ L borate buffer (0.2 M boric acid, pH 8.8) and then derivatized with 20 μ L AQC (fluorescent reagent 6-amino-quinolyl-*N*-hydroxy succinimidyl carbamate; Watrex, Prague, Czech Republic). The quantification of the amino acids was carried out with appropriate standard curves in an HPLC system consisting of a P680 HPLC Dionex pump, ASI 100 Dionex autosampler, RF 2000 fluorescence detector, UCI 50 Dionex interface, and a UVD 170 U Dionex UV detector. Nucleodur cc 250/4 100-5 c18ec served as the HPLC column. Aliquots of 25 μ L were heated to 37°C on an autosampler and 20 μ L were applied to the column by a pump, with a flow rate of 1 mL/min. The chromatograms were evaluated using the software Chromeleon version 6.7 (ThermoFisher, Waltham, MA, USA).

Determination of vitamin B₆

Vitamin B₆ extraction was performed and analyzed as described previously (Colinas et al., 2016) with the following changes: two separate extractions were performed, one with 16 volumes (extraction 1) and one with 8 volumes (extraction 2) of 50 mM ammonium acetate (pH 4.0), respectively. A 50- μ L injection volume was used for a single run per extract. The calculations of PMP, PLP, and PL were based on extraction 1 while the calculations of PM and PN were based on extraction 2.

Heterologous expression of *AtPLPP1* in *E. coli*

Heterologous *AtPLPP1* expression was performed using the isopropyl- β -D-thiogalactopyranoside-inducible T7 RNA polymerase pET-vector/Rosetta 2 (DE3) expression system (Merck Biosciences, Novagen, Darmstadt, Germany). For this, the coding sequence of *AtPLPP1* was amplified from Arabidopsis leaf cDNA with the following primer combination: PLPP_NdeI_fwd: NNNCATATGACTTTCCTTATCAA GAACATTTATTTC, PLPP_BamHI_rev NNN GGATCCCTAC GGGTTCAGGTCGAAGTTCGTCTCC, allowing in-frame insertion (via the *NdeI* and *BamHI* restriction sites) with the His-tag sequence of the pET16b vector. The correctness of the expression construct was verified by Sanger sequencing. Rosetta 2 cells containing the expression construct were cultivated in 50 mL standard YT media (0.8% [w/v] peptone, 0.5% [w/v] yeast extract, 0.25% [w/v] NaCl, pH 7.0) at 37°C aerobically overnight. From this culture, a new culture was started under the same condition. At an optical density of 0.2 at 600 nm, growth of the culture was continued aerobically at 15°C. At OD₆₀₀ = 0.5, recombinant protein synthesis was induced by the addition of 1 mM isopropyl- β -D-

thiogalactopyranoside, and the cells were harvested the next day by centrifugation (5 min; 5,000 × g). Cell disruption, protein purification, and immunostaining were performed as previously described (Trentmann et al., 2007). However, in contrast to Trentmann et al. (2007), the soluble fraction was used for protein enrichment via IMAC.

Phosphatase assay

The biochemical characterization of the purified HAD-type phosphatase AtPLPP1 was assayed as described previously (Sussman and Avron, 1981). The reaction mixture used contained 20 mM Tris–HCl pH 7.0, 5 mM MgCl₂, and the tested substrates (in the given concentrations) in a total volume of 0.5 mL at 23°C. Approximately 6.25 μg/0.5 mL of purified protein was used in each enzymatic reaction. Reactions were stopped by adding perchloric acid to the reaction mixture (4.5% [v/v]). Subsequently, 200 μL of the mixture was used for phosphate determination using a standardized colorimetric assay (Ames, 1966).

GFP localization studies

To analyze the subcellular localization of AtPLPP1 in *Arabidopsis* and *N. benthamiana*, AtPLPP1–GFP fusion constructs were generated using the Gateway destination vectors pK7FWG2 (Karimi et al., 2002) for GFP attached to the C-terminus of AtPLPP1 and pK7WGF2 (Karimi et al., 2002) for an N-terminal fusion construct. For this, cDNA of AtPLPP1 was amplified omitting the stop codon via PCR using PLPP-specific primers (PLPP_fwd: ggggacaagttgtacaaaaaagcaggcttaATGACTTTCCTCTTATCAAGAACATTTATTCTCT CAC, PLPP_rev_+ stop: ggggaccactttgtacaagaagctgggttCTACGGGTTTCAGGTCGAAGTT PLPP_rev_-stop: ggggaccactttgtacaagaagctgggttCGGGTTCAGGTCGAAGTTTCG), and including the *attB1* and *attB2* sites (lower case letters of the sequences). The amplified sequence was cloned into the entry vector pDONR_{ZEO} (Invitrogen) via the BP reaction and subsequently by an LR reaction into the respective destination vector. Protoplasts from mesophyll cells were isolated and transiently transformed according to Yoo et al. (2007). For imaging, a Leica TCS SP5 II confocal laser-scanning microscope was used (Objective: HCX PL APO lambda blue 63.0 × 1.20 WATER UV; Excitation wavelength laser: 488 nm Argon laser; Filter bandwidth emission: 495–540 nm [GFP], 651–704 nm [chloroplasts autofluorescence]).

Statistical analyses

Leaves or total rosettes from individual plants of the same age were used in physiological studies and acted as replicates. To determine the significance level of the mean of two sample sets (wt data or *er-ant1* data were taken as reference) one-tailed Student's *t* tests were used. Prior to the statistical analysis, normal distribution of data and equality of the variances were analyzed.

Accession numbers

Sequence data from this article can be found in the GenBank/EMBL data libraries under accession numbers:

At5g17400 (ER-ANT1), At2g33255 (AtPLPP1), YOR131C (PLPP_Sc from baker's yeast), and At2g28330 (SAND house-keeping gene). AOA1S3ZWH3_TOBAC (*NtPLPP1*).

Supplemental data

The following materials are available in the online version of this article.

Supplemental Figure S1. SNP induced changes in the At2g33255 gene product.

Supplemental Figure S2. Confirmation of the candidate SNP in At2g33255 of *ser-ant1* line 6.3.

Supplemental Figure S3. Analysis of At2g33255 T-DNA insertion lines.

Supplemental Figure S4. Analysis of *promHAD1::HAD1 x had1-2 x er-ant1* and *ubiq::HAD1 x had1-2 x erant1* lines.

Supplemental Figure S5. ClustalW alignment of the amino acid sequences of the PLPP from *N. tabacum* (*NtPLPP1*) and the At2g33255 gene product.

Supplemental Figure S6. Purification of the HAD-type hydrolase, At2g33255, heterologously expressed in *E. coli* Rosetta cells.

Supplemental Table S1. SNP in the coding sequence of At2g33255 from different *er-ant1* suppressor lines.

Acknowledgments

We are grateful to Jochen Wartenberg for excellent photography (Supplemental Figure S4).

Funding

Work in the lab of H.E.N. was financially supported by the Deutsche Forschungsgemeinschaft (DFG, Project NE 418/19-1). Cooperation between H.E.N., D.L., and T.K. was funded by the DFG in the frame of the TRR175 (projects B03, C05. and C01). T.B.F. would like to gratefully acknowledge funding from the Swiss National Science Foundation (Grants 31003A-141117/1 and 310030-192466).

Conflict of interest statement. None declared.

References

- Ames BN (1966) Assay of inorganic phosphate, total phosphate and phosphatases. In EF Neufeld, V Ginsburg, eds, *Methods in Enzymology*, Vol VIII. Academic Press, New York, NY
- Barton DA, Cole L, Collings DA, Liu DYT, Smith PMC, Day DA, Overall RL (2011) Cell-to-cell transport via the lumen of the endoplasmic reticulum. *Plant J* **66**: 806–817
- Bauwe H, Hagemann M, Fernie AR (2010) Photorespiration: players, partners and origin. *Trends Plant Sci* **15**: 330–336
- Burroughs AM, Allen KN, Dunaway-Mariano D, Aravind L (2006) Evolutionary genomics of the HAD superfamily: Understanding the structural adaptations and catalytic diversity in a superfamily of phosphoesterases and allied enzymes. *J Mol Biol* **361**: 1003–1034
- Caparrós-Martín JA, McCarthy-Suárez I, Culiñez-Macià FA (2013) HAD hydrolase function unveiled by substrate screening: Enzymatic characterization of *Arabidopsis thaliana* subclass I phosphosugar phosphatase AtSgpp. *Planta* **237**: 943–954
- Clairemont CA, De Maio A, Hirschberg CB (1992) Translocation of ATP into the lumen of rough endoplasmic reticulum-derived

- vesicles and its binding to luminal proteins including BiP (GRP 78) and GRP 94. *J Biol Chem* **267**: 3983–3990
- Colinas M, Eisenhut M, Tohge T, Pesquera M, Fernie AR, Weber APM, Fitzpatrick TB** (2016) Balancing of B₆ vitamers is essential for plant development and metabolism in Arabidopsis. *Plant Cell* **28**: 439–453
- Corso M, Doccua FG, de Melo JRF, Costa A, Verbruggen N** (2018) Endoplasmic reticulum-localized CCX2 is required for osmotolerance by regulating ER and cytosolic Ca²⁺ dynamics in Arabidopsis. *Proc Natl Acad Sci USA* **115**: 3966–3971
- Demmig B, Björkman O** (1987) Comparison of the effect of excessive light on chlorophyll fluorescence (77K) and photon yield of O₂ evolution in leaves of higher plants. *Planta* **171**: 171–184
- Douce R, Bourguignon J, Neuburger M, Rebeille F** (2001) The glycine decarboxylase system: A fascinating complex. *Trends Plant Sci* **6**: 167–176
- Eliot AC, Kirsch JF** (2004) Pyridoxal phosphate enzymes: Mechanistic, structural, and evolutionary considerations. *Ann Rev Biochem* **73**: 383–415
- Etherington GJ, Monaghan J, Zipfel C, MacLean D** (2014) Mapping mutations in plant genomes with the userfriendly web application CandiSNP. *Plant Meth* **10**: 41
- Fitzpatrick TB, Amrhein N, Kappes B, Macheroux P, Tews I, Raschle T** (2007) Two independent routes of de novo vitamin B₆ biosynthesis: Not that different after all. *Biochem J* **407**: 1–13
- Friml J, Jones AR** (2010) Endoplasmic Reticulum: the rising compartment in auxin biology. *Plant Physiol* **154**: 458–462
- Gallii G, Sengupta-Gopalan C, Ceriotti A** (1998) The endoplasmic reticulum of plant cells and its role in protein maturation and biogenesis of oil bodies. *Plant Mol Biol* **38**: 1–29
- Geigenberger P, Riewe D, Fernie AR** (2010) The central regulation of plant physiology by adenylates. *Trends Plant Sci* **15**: 98–105
- González E, Danehower D, Daub ME** (2007) Vitamer levels, stress response, enzyme activity, and gene regulation of Arabidopsis lines mutant in the pyridoxine/pyridoxamine 5'-phosphate oxidase (PDX3) and the pyridoxal kinase (SOS4) genes involved in the vitamin B₆ salvage pathway. *Plant Physiol* **145**: 985–996
- Guillén E, Hirschberg CB** (1995) Transport of adenosine triphosphate into the endoplasmic reticulum proteoliposomes. *Biochemistry* **34**: 5472–5476
- Haferkamp I, Fernie AR, Neuhaus HE** (2011) Adenine nucleotide transport in plants: much more than a mitochondrial issue. *Trends Plant Sci* **16**: 507–515
- Haferkamp I, Schmitz-Esser S** (2012) The plant mitochondrial carrier family: Functional and evolutionary aspects. *Front Plant Sci* **3**: 2
- Heineke D, Bykova N, Gardestrom P, Bauwe H** (2001) Metabolic response of potato plants to an antisense reduction of the P-protein of glycine decarboxylase. *Planta* **212**: 880–887
- Helliwell C** (2006) The ER and plant hormones. In DG Robinson, ed., *The Plant Endoplasmic Reticulum*. Springer, Berlin, Heidelberg, pp 233–249
- Hellmann H, Mooney S** (2010) Vitamin B₆: a molecule for human health? *Molecules* **15**: 442–459
- Hoffmann C, Plochanski B, Haferkamp I, Leroch M, Ewald R, Bauwe H, Riemer J, Herrmann JM, Neuhaus HE** (2013) From endoplasmic reticulum to mitochondria: Absence of the Arabidopsis ATP antiporter Endoplasmic Reticulum Adenylate Transporter1 perturbs photorespiration. *Plant Cell* **25**: 2647–2660
- James GV, Patel V, Nordström KJV, Klases JR, Salomé PA, Weigel D, Schneeberger K** (2013) User guide for mapping-by-sequencing in Arabidopsis. *Genome Biol* **14**: R61–R61
- Ju C, Yoon GM, Shemansky JM, Lin DY, Ying ZI, Chang J, Garrett WM, Kessenbrock M, Groth G, Tucker ML, et al.** (2012) CTR1 phosphorylates the central regulator EIN2 to control ethylene hormone signaling from the ER membrane to the nucleus in Arabidopsis. *Proc Natl Acad Sci USA* **109**: 19486–19491
- Karimi M, Inze D, Depicker A** (2002) GATEWAY vectors for Agrobacterium-mediated plant transformation. *Trends Plant Sci* **7**: 193–195
- Karley AJ, White PJ** (2009) Moving cationic minerals to edible tissues: Potassium, magnesium, calcium. *Curr Opin Plant Biol* **12**: 291–298
- Keys A** (2006) The re-assimilation of ammonia produced by photorespiration and the nitrogen economy of C3 higher plants. *Photosynth Res* **87**: 165–175
- Kim Y, Schumaker KS, Zhu JK** (2006) EMS mutagenesis of Arabidopsis. *Methods Mol Biol* **323**: 101–103
- Klein MC, Zimmermann K, Schorr S, Landini M, Klemens PAW, Altensell J, Jung M, Krause E, Nguyen D, Helms V, et al.** (2018) AXER is an ATP/ADP exchanger in the membrane of the endoplasmic reticulum. *Nat Commun* **9**: 3489
- Klingenberg M** (1989) Molecular aspects of adenine nucleotide carrier from mitochondria. *Arch Biochem Biophys* **270**: 1–14
- Koonin EV, Tatusov RL** (1994) Computer analysis of bacterial haloacid dehalogenases defines a large superfamily of hydrolases with diverse specificity: application of an iterative approach to database search. *J Mol Biol* **244**: 125–132
- Krishnakumar V, Hanlon MR, Contrino S, Ferlanti ES, Karamycheva S, Kim M, Rosen BD, Cheng C-Y, Moreira W, Mock SA, et al.** (2014) Araport: the Arabidopsis information portal. *Nucl Acids Res* **43**: D1003–D1009
- Kuznetsova E, Nocek B, Brown G, Makarova KS, Flick R, Wolf YI, Khusnutdinova A, Evdokimova E, Jin K, Tan K, et al.** (2015) Functional diversity of haloacid dehalogenase superfamily phosphatases from *Saccharomyces cerevisiae*: Biochemical, structural, and evolutionary insights. *J Biol Chem* **290**: 18678–18698
- Leroch M, Neuhaus HE, Kirchnerberger S, Zimmermann S, Melzer M, Gerhold J, Tjaden J** (2008) Identification of a novel adenine nucleotide transporter in the endoplasmic reticulum of Arabidopsis. *Plant Cell* **20**: 438–451
- Li H, Handsaker B, Wysoker A, Fennell T, Ruan J, Homer N, Marth G, Abecasis G, Durbin R, Subgroup GPDP** (2009) The sequence alignment/map format and SAMtools. *Bioinformatics* **25**: 2078–2079
- Livak KJ, Schmittgen TD** (2001) Analysis of relative gene expression data using real-time quantitative PCR and the 2^{-ΔΔCT} method. *Methods* **25**: 402–408
- Lui A, Lumeng L, Li TK** (1981) Metabolism of vitamin B₆ in rat liver mitochondria. *J Biol Chem* **256**: 6041–6046
- Lui A, Lumeng L, Li TK** (1982) Transport of pyridoxine and pyridoxal 5'-phosphate in isolated rat liver mitochondria. *J Biol Chem* **257**: 14903–14906
- Mayinger P, Meyer DI** (1993) An ATP transporter is required for protein translocation into the yeast endoplasmic reticulum. *EMBO J* **12**: 659–666
- Millar AH, Heazlewood JL** (2003) Genomic and proteomic analysis of mitochondrial carrier proteins in Arabidopsis. *Plant Physiol* **131**: 443–453
- Mitchell AL, Attwood TK, Babbitt PC, Blum M, Bork P, Bridge A, Brown SD, Chang H-Y, El-Gebali S, Fraser MI, et al.** (2018) InterPro in 2019: Improving coverage, classification and access to protein sequence annotations. *Nucleic Acids Res* **47**: D351–D360
- Möhlmann T, Steinebrunner I, Neuhaus HE** (2014) Nucleotides and nucleosides: transport, metabolism and signaling function of extracellular ATP. In U Lüttge, W Beyschlag, JC Cushman, eds, *Prog. Bot.* Vol 75. Springer, Heidelberg, Germany, pp 119–144
- Oda K, Kamiya T, Shikanai Y, Shigenobu S, Yamaguchi K, Fujiwara T** (2016) The Arabidopsis Mg transporter, MRS2-4, is essential for Mg homeostasis under both low and high Mg conditions. *Plant Cell Physiol* **57**: 754–763
- Oliver DJ, Neuburger M, Bourguignon J, Douce R** (1990) Interaction between the component enzymes of the glycine decarboxylase multienzyme complex. *Plant Physiol* **94**: 833–839

- Pallotta MA, Graham RD, Langridge P, Sparrow DHB, Barker SJ** (2000) RFLP mapping of manganese efficiency in barley. *Theor Appl Genet* **101**: 1100–1108
- Parra M, Stahl S, Hellmann H** (2018) Vitamin B₆ and its role in cell metabolism and physiology. *Cells* **7**: 84
- Porra RJ** (2002) The chequered history of the development and use of simultaneous equations for the accurate determination of chlorophylls a and b. *Photosynth Res* **73**: 149–156
- Reinhold T, Alawady A, Grimm B, Beran KC, Jahns P, Conrath U, Bauer J, Reiser J, Melzer M, Jeblick W, et al.** (2007) Limitation of nocturnal import of ATP into *Arabidopsis* chloroplasts leads to photooxidative damage. *Plant J* **50**: 293–304
- Reiser J, Linka N, Lemke L, Jeblick W, Neuhaus HE** (2004) Molecular physiological analysis of the two plastidic ATP/ADP transporters from *Arabidopsis thaliana*. *Plant Physiol* **136**: 3524–3536
- Reyes-Prieto A, Moustafa A** (2012) Plastid-localized amino acid biosynthetic pathways of *Plantae* are predominantly composed of non-cyanobacterial enzymes. *Sci Rep* **2**: 955–955
- Roux SJ, Steinebrunner I** (2007) Extracellular ATP: an unexpected role as a signaler in plants. *Trends Plant Sci* **12**: 522–527
- Rueschhoff E, Gillikin J, Sederoff H, Daub M** (2012) The SOS4 pyridoxal kinase is required for maintenance of vitamin B₆-mediated processes in chloroplasts. *Plant Physiol Biochem* **63C**: 281–291
- Sato S, Yanagisawa S** (2014) Characterization of metabolic states of *Arabidopsis thaliana* under diverse carbon and nitrogen nutrient conditions via targeted metabolomic analysis. *Plant Cell Physiol* **55**: 306–319
- ShuoHao H, Jing L, Jie Z, JianYun Z, LongQuan H** (2019) Identification and characterization of a pyridoxal 5'-phosphate phosphatase in tobacco plants. *Plant Sci* **278**: 88–95
- Song J, Li Z, Liu Z, Guo Y, Qiu LJ** (2017) Next-generation sequencing from bulked-segregant analysis accelerates the simultaneous identification of two qualitative genes in soybean. *Front Plant Sci* **8**: 919
- Sussman I, Avron M** (1981) Characterization and partial purification of dl-glycerol-1-phosphatase from *Dunaliella salina*. *Biochim Biophys Acta* **661**: 199–204
- Tambasco-Studart M, Titiz O, Raschle T, Forster G, Amrhein N, Fitzpatrick TB** (2005) Vitamin B₆ biosynthesis in higher plants. *Proc Natl Acad Sci USA* **102**: 13687–13692
- Timm S, Florian A, Fernie AR, Bauwe H** (2016) The regulatory interplay between photorespiration and photosynthesis. *J Exp Bot* **67**: 2923–2929
- Timm S, Mielewczik M, Florian A, Frankenbach S, Dreissen A, Hocken N, Fernie AR, Walter A, Bauwe H** (2012) High-to-low CO₂ acclimation reveals plasticity of the photorespiratory pathway and indicates regulatory links to cellular metabolism of *Arabidopsis*. *PLoS ONE* **7**: e42809
- Tjaden J, Möhlmann T, Kampfenkel K, Henrichs G, Neuhaus HE** (1998) Altered plastidic ATP/ADP-transporter activity influences potato (*Solanum tuberosum*) tuber morphology, yield and composition of tuber starch. *Plant J* **16**: 531–540
- Trentmann O, Horn M, van Scheltinga AC, Neuhaus HE, Haferkamp I** (2007) Enlightening energy parasitism by analysis of an ATP/ADP transporter from chlamydiae. *PLoS Biol* **5**: e231
- Trentmann O, Jung B, Neuhaus HE, Haferkamp I** (2008) Non-mitochondrial ATP/ADP transporters accept phosphate as third substrate. *J Biol Chem* **283**: 36486–36493
- Weigel D, Glazebrook J** (2002) *Arabidopsis*. In *A Laboratory Manual*. Cold Spring Harbor Laboratory Press, New York, NY [Database]
- Whittaker MM, Penmatsa A, Whittaker JW** (2015) The Mtm1p carrier and pyridoxal 5'-phosphate cofactor trafficking in yeast mitochondria. *Arch Biochem Biophys* **568**: 64–70
- Winkler HH, Neuhaus HE** (1999) Non-mitochondrial ATP transport. *Trends Biochem Sci* **24**: 64–68
- Winter G, Todd CD, Trovato M, Forlani G, Funck D** (2015) Physiological implications of arginine metabolism in plants. *Front Plant Sci* **6**: 534–534
- Wulfetange K, Lomin SN, Romanov GA, Stolz A, Heyl A, Schmülling T** (2011) The cytokinin receptors of *Arabidopsis* are located mainly to the endoplasmic reticulum. *Plant Physiol* **156**: 1808–1818
- Yoo SD, Cho YH, Sheen J** (2007) *Arabidopsis* mesophyll protoplasts: A versatile cell system for transient gene expression analysis. *Nat Protoc* **2**: 1565–1572
- Zhang X, Zheng X, Ke S, Zhu H, Liu F, Zhang Z, Peng X, Guo L, Zeng R, Hou P, et al.** (2016) ER-localized adenine nucleotide transporter ER-ANT1: An integrator of energy and stress signaling in rice. *Plant Mol Biol* **92**: 701–715